A Physical and Versatile Aging Compact Model for Hot Carrier Degradation in SiGe HBTs under Dynamic Operating Conditions

C. Mukherjee[a], F. Marc[a], M. Couret[a], G. G. Fischer[b], M. Jaoul[a,c], D. Céli[c], K. Aufinger[d], T. Zimmer[a] and C. Maneux[a]

[a]*IMS Laboratory, University of Bordeaux, UMR CNRS 5218, Cours de la Libération - 33405 Talence, France*
[b]*IHP, Leibniz-Institut für innovative Mikroelektronik, 15236 Frankfurt (Oder), Germany*
[c]*STMicroelectronics, 38926 Crolles, France*
[d]*Infineon Technologies AG, 81726 Munich, Germany*

Abstract

This paper presents a new physics-based compact model implementation for interface state creation due to hot-carrier degradation in advanced SiGe HBTs. This model accounts for dynamic stress bias conditions through a combination of the solution of reaction-diffusion theory and Fick's law of diffusion. The model reflects transistor degradation in terms of base recombination current parameters of HiCuM compact model and its accuracy has been validated against results from long-term DC and dynamic aging tests performed close to the safe-operating-areas of various HBT technologies.

Keywords: Aging; Aging tests, compact model, hot-carrier degradation, safe operating area, SiGe HBTs.

*Corresponding author
E-mail address:*chhandak.mukherjee@ims-bordeaux.fr (C. Mukherjee)

1

A Physical and Versatile Aging Compact Model for Hot Carrier Degradation in SiGe HBTs under Dynamic Operating Conditions

C. Mukherjee[a], F. Marc[a], M. Couret[a], G. G. Fischer[b], M. Jaoul[a,c], D. Céli[c], K. Aufinger[d], T. Zimmer[a] and C. Maneux[a]

[a]*IMS Laboratory, University of Bordeaux, UMR CNRS 5218, Cours de la Libération - 33405 Talence, France*
[b]*IHP, Leibniz-Institut für innovative Mikroelektronik, 15236 Frankfurt (Oder), Germany*
[c]*STMicroelectronics, 38926 Crolles, France*
[d]*Infineon Technologies AG, 81726 Munich, Germany*

1. Introduction

Aggressive miniaturization of SiGe heterojunction bipolar transistors (HBTs) has enhanced the frequency performances of the transistors while increasing the operating current density and sacrificing breakdown voltages [1]. This has posed as a major concern in terms of long-term reliability since modern transistors are required to operate closer and even beyond their classical safe-operating areas (SOA) thus shortening the transistor's lifetime. This is only possible, if the underlying physical processes of degradation are well understood and accurately modeled. One of the major reliability issues is hot-carrier degradation (HCD) that predominantly limits the lifetimes of modern SiGe HBTs [2-6], the underlying mechanism of which is trap generation at the emitter-base (EB) spacer oxide interface through Si-H bond-breaking followed by non-ideal base current degradation [2]. Despite the criticism put forward against reaction–diffusion (R–D) theory, it has remained a well-accepted modeling framework over the years for understanding HCD [2-12]. In the context of modern HBTs, R-D theory remains valid [2, 12] owing to the fact that recovery is quite scarce under conventional operating conditions (since interface traps do not recover significantly without annealing). Moreover, the analytic form of R-D model is quite suitable for circuit design while preserving the physical basis of

degradation [9]. In compact model implementation, an approximate solution of the R-D rate equation is commonly used in which the time-dependence of the degradation is governed by a power law (t^n) [7-8, 11-12]. Though it offers simplicity, this power law does neither account for the saturation of the degradation characteristics after long-term aging (when the trap density approaches the total number of available dangling bonds), nor for the initial phase when the generation process dominates ($\sim t$). Other solutions include an empirical time dependence of the power law exponent by Fischer *et al.* [3-4] or an exponential model for trap density in [5], based on the R-D model, however omitting trap annihilation. To circumvent specific limitations of all these models, a complete analytical solution of the R-D model has also been proposed [2] which captures all phases of degradation in one single analytic form, thus enabling physics-based compact modeling owing to its design-friendly implementation. However, this model, though comprehensive and accurate in all other aspects, does not account for a dynamic stress condition, *i.e.*, the invariance in time is not preserved for the degradation in case of variable stress bias intervals, which is an essential criterion for AC circuit simulation [13]. Consider for example the scenario illustrated in Fig. 1 for the base recombination current parameter at the base-emitter periphery, I_{REpS}, extracted from measurements under a dynamic stress bias condition (switching between two stress biases). In the first interval, between (0-t_1), previous implementation [2] (HiCuM AL-V1) follows the actual measurements. However, between t_1 and t_2, *i.e.* under the low stress condition, the

*Corresponding author
E-mail address:*chhandak.mukherjee@ims-bordeaux.fr (C. Mukherjee)

previous implementation calculates the degradation according to the new stress bias without retaining the final value of I_{REpS} from the first (high) stress phase, thus leading to a discontinuity compared to the measured data which shows a weak recovery under low-stress conditions.
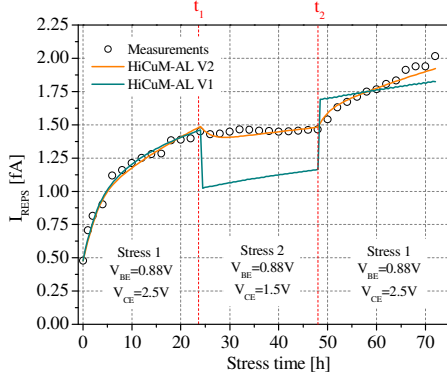

Fig. 1: Impact of variable stress condition on base current recombination parameter, I_{REpS}, comparing the measurements, previous and newly proposed implementations.

It is to be noted that, one cannot directly transpose a model with both constant and variable stress types as long as the model accounts for recovery and non-quasi-static behavior of the dynamic stress [13]. Hence, to circumvent this problem, a new implementation is proposed in this work to account for dynamic stress conditions, while preserving the same R-D model framework as before [2]. In Fig.1, corresponding new model (to be detailed in the next section) simulation (HiCuM AL-V2) is illustrated showing a much better agreement with the measurements under variable stress conditions.

The rest of this paper is organized as follows; Section II illustrates the model formulation and implementation; Section III describes the three SiGe HBT technologies under test and their respective stress bias conditions, the aging test results, model validation and a discussion on the evolution of aging model parameters with bias followed by the conclusion.

2. Implementation of the Aging Model

The schematic in Fig. 2 illustrates the spatial dynamics of hydrogen diffusion in the emitter-base spacer oxide due to the hot-carrier-induced degradation in SiGe HBTs and the subsequent Si-H bond breakage at the [2-8,14] oxide interface.
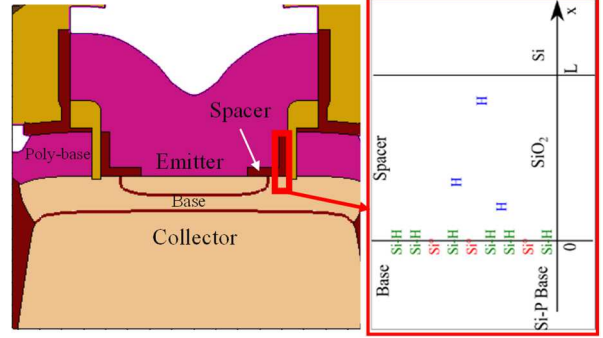

Fig. 2: Schematic of the hydrogen diffusion model considering the interface between the base and the EB-spacer; L is the E-B spacer thickness.

The rate of bond dissociation is governed by a chemical interaction between the carriers and the passivated Si-H bond through generation and annihilation of traps. The interface-trap density, N_T (t), increases with the net rate of reaction, g_T (t), which is described by the R-D model [2, 10] as,

$$g_T(t) = K_F(N_F - N_T(t)) - K_R N_T(t) N_H(0,t) \quad (1)$$

Here, K_F is the rate constant of the forward reaction, *i.e.*, generation of traps, K_R is the rate constant of trap annihilation by hydrogen atoms, $N_H(x,t)$ is the volumetric density of hydrogen at distance x of the Si/SiO$_2$ interface and N_F is the total number of available bonds that can break. When a Si–H breaks, every dangling Si bond is associated with a free H atom in the oxide [11], hence,

$$g_T(t) = \frac{dN_T}{dt} = \Phi_H(0,t) \quad (2)$$

where $\Phi_H(x,t)$ is the surface flow density of hydrogen. In the oxide volume, the flow of hydrogen is related to the density by Fick's law of diffusion:

$$\Phi_H(x,t) = -D_H \frac{\partial N_H(x,t)}{\partial x} \quad (3)$$

where D_H is the diffusion constant of hydrogen. Adding the hydrogen conservation law when x>0, Fick's second law reads,

$$\frac{\partial N_H(x,t)}{\partial t} - D_H \frac{\partial^2 N_H(x,t)}{\partial x^2} = 0 \quad (4)$$

In order to introduce in the compact model the time-invariance property and the memory effect necessary for dynamic stress simulation, we introduce a new structure of the compact model compared to [2], and

3

especially the diffusion model implementation (Fig. 3). Equations (1) and (2) can be directly embedded in a Verilog-A model, resulting in relations between $g_T(t), \Phi_H(0,t), N_T(t)$ and $N_H(0,t)(= N_{H0}(t))$ along with their time derivatives, all of them being located at the interface (x=0). This part of the model interacts with the electrical part of the model through K_F and K_R as inputs, and through the trap density $N_T(t)$ as an output. In the previous version [2], the aging model (HiCuM-AL) had been implemented in HiCuM compact model [15] through the recombination current parameter in the periphery, I_{REpS}, featuring a similar evolution as the trap density $N_T(x, t)$. Hence, in the the aging model (HiCuM-AL v2), K_F (s^{-1}), K_R (cm^{3}s^{-1}) are represented by their corresponding compact model parameters $K_{F,I}$ (s^{-1}), $K_{R,I}$ (cm.A^{-1}·s^{-1}), respectively, and N_F by I_F (A) which is the final value of ΔI_{REpS}, (A).
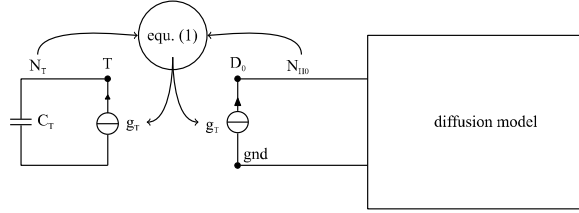

Fig. 3: Organization of the R-D and Diffusion model implementation.

The rest of the system is modeled by the diffusion equations in the oxide volume or at the interface. The diffusion model cannot directly be implemented in Verilog-A. However, there is no need to implement the complete equations but only to identify the relation between $N_H(0,t)$ and $g_T(t)$, i.e. $\Phi_H(,t)$. Moreover, diffusion being a linear and time-invariant phenomenon, its useful properties can be summarized by the equivalent admittance-like quantity defined as $\tilde{Y}_H(0,f) = \tilde{\Phi}_H(0,f)/\tilde{N}_H(0,f)$, where $\tilde{N}_H(x,f)$ and $\tilde{\Phi}_H(x,f)$ are the Fourier transforms of $N_H(x,t)$ and $\Phi_H(x,t)$. In order to simulate the diffusion model in a Spice-like circuit simulator, it must be organized around a finite set of nodes or variables. To obtain a time-invariant model, the time must not appear explicitly in the equations but only in time derivatives. The distributed partial derivative equations will be replaced by a finite set of first order differential equations implemented by a resistor-capacitor (R-C) network. As the physical system can only be considered for one dimension, an R-C ladder network is used. This architecture is commonly used for thermal diffusion modeling [16]. It is made of N

resistors and N capacitors followed by an optional terminal resistor (of conductance G) depicted in Fig.4.
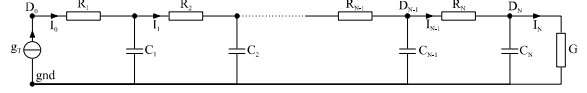

Fig. 4: R-C ladder network representing Hydrogen diffusion model.

The node D_0 is the input of the circuit. For an easier conversion to Verilog-A model, hydrogen flow density is presented as currents I_N (ensuring conservation law) and hydrogen density as potential V_N at node D_N. The voltage at D_0 is $V_0 = N_H(0,t)$. The input current is $I_0 = \Phi_H(0,t) = g_T(t)$. In frequency representation, introducing admittances $\tilde{Y}_n = \tilde{I_N}/\tilde{V_N}$, we have the recurrence:

$$\tilde{Y}_N = G$$
$$\tilde{Y}_{n-1} = \frac{1}{R_n + \frac{1}{j2\pi f C_n + \tilde{Y}_n}} ; n = 1..N \quad (5)$$

In order to reduce the number of parameters added to our model, the values of R_n and C_n follow two geometrical sequences:

$$R_n = R_1 \alpha_R^{n-1}, \quad C_n = C_1 \alpha_C^{n-1} \quad (6)$$

This sequence can be identified to a finite difference approximation along the x axis depicted in Fig. 2, considering a geometrically increasing sequence of x. Owing to a one dimensional system, both sequences must have the same common ratio $\alpha_R = \alpha_C$. To identify the diffusion compact model parameters, we need to compare them with the ones of the diffusion model equations. For this, the Fick's second law is translated into the frequency domain as:

$$\frac{\partial^2 \tilde{N_H}(x,f)}{\partial x^2} - j\frac{2\pi f}{D_H}\tilde{N_H}(x,f) = 0 \quad (7)$$

whose general solution is $\tilde{N_H}(x,f) = A_H e^{\alpha x} + B_H e^{-\alpha x}$ with $\alpha = (1+j)\sqrt{\frac{\pi f}{D_H}}$. Hence, Fick's first law, which reads,

$$\tilde{\Phi_H}(x,f) = -D_H\frac{\partial \tilde{N_H}(x,f)}{\partial x} \quad (8)$$

becomes, $\tilde{\Phi_H}(x,f) = -\alpha D_H(A_H e^{\alpha x} - B_H e^{-\alpha x})$ \quad (9)

Coefficients A_H and B_H are determined by the limit conditions at the interfaces $x = 0$ and $x = L$ as

4

represented in Fig. 2. Considering the limits at $x=0$, we obtain the following relationships:

$$\widetilde{N_H}(0,f) = A_H + B_H \qquad (10)$$
$$\widetilde{\Phi_H}(0,f) = -(1+j)\sqrt{\pi f D_H}(A_H - B_H)$$

and for $x = L$:

$$\widetilde{N_H}(L,f) = (A_H e^{\alpha L} + B_H e^{-\alpha L}) \qquad (11)$$
$$\widetilde{\Phi_H}(L,f) = -(1+j)\sqrt{\pi f D_H}(A_H e^{\alpha L} - B_H e^{-\alpha L})$$

Accordingly, the three limit conditions of the diffusion admittance-like quantity $\tilde{Y}(f)$ are summarized in Table I: one for very thick oxide, and two for finite thickness. Parameter values can be derived from the R-C network configuration. At high frequency, the network is equivalent to the R_1 resistor. For $\alpha_R > 1$, the limit frequency is:

$$f_1 = \frac{1}{2\pi R_1 C_1} \qquad (12)$$

By identifying $1/R_1 \approx |\tilde{\Phi}(0,f_1)|$ for the semi-infinite exact model, we derive

$$R_1 \approx \frac{1}{\sqrt{2\pi f_1 D_H}} \text{ and } C_1 \approx R_1 D_H \qquad (13)$$

We can now approximate R_1 and C_1 on the basis of the diffusion coefficient D_H and the maximum frequency f_1 for the validity of the R-C network approximation. On the other hand, the minimum accurate frequency of the RC model is approximated by the cut-off frequency of the last cell:

$$f_N \approx \frac{1}{2\pi R_N C_N} = \frac{f_1}{\alpha_R^{(2N-2)}} \qquad (14)$$

The effective values of the number of R-C cells, N, and $\alpha_R = \alpha_C$ are adjusted using (14), and by taking into account the desired accuracy/complexity trade-off. Finally, the terminal conductance G is chosen to adjust the long term behavior of the model and the nature of the second interface on the other side of the spacer. In Figure 5 the Bode-like representation of normalized admittance $\tilde{Y}(f)$ as a function of frequency f is drawn using the quantities:

$$f_0 \simeq \frac{D_H}{2\pi L^2} \text{ and } Y_0 \simeq \frac{D_H}{L} \qquad (15)$$

We observe that all models have identical behavior for frequencies between $f_N = f_0$ and f_1 following a $\sqrt{f}$ law, characteristic of diffusion. We observe that the R-C model fits well approximately for 4 decades using a 5 R-C cell network with a slight offset. Hence this 5-cell configuration was chosen as optimum (accuracy vs. complexity) for further analysis.
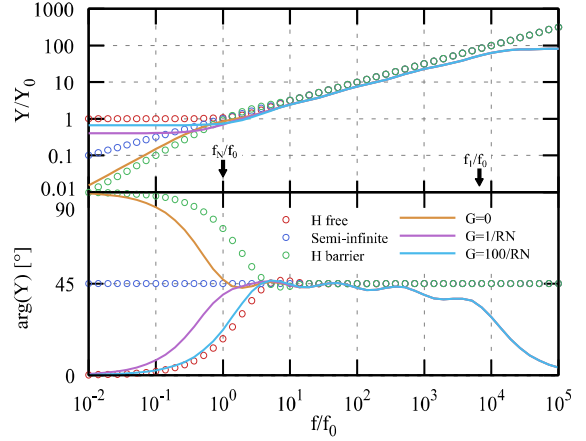

Fig. 5: Bode-like representation of normalized "Admittance" $\tilde{Y}(f)/Y_0$ of diffusion through oxide for the theoretical model (symbols, three cases according to second interface properties) and for the RC-ladder (lines) model for $\alpha_R = 3$ and $N = 5$; Arrows indicating the domain of validity.

3. Stress Conditions and Model Validation

While the new implementation ensures model validity under dynamic stress (Fig. 1), in this section, we test the versatility of the model under various aging conditions, close to the SOA of the transistors, through comparison between the aging model simulation and results of aging tests on three different advanced SiGe HBT technologies. We present the details of the extracted parameters pertaining to the model HiCuM-AL V2 in Table II for the SiGe HBTs under study.

3.1 Technology 1

Aging-tests were performed on SiGe NPN HBTs from Infineon Technologies [2, 5]. The DUTs of drawn emitter dimension 0.2×10 μm² exhibit peak f_T/f_{MAX} of 240/380 GHz and a BV_{CE0} of 1.3V. Details

TABLE I: LIMIT CONDITIONS FOR HYDROGEN DIFFUSION MODEL

Limit conditions		$\tilde{Y}(f) = \widetilde{\Phi_H}(0,f)/\widetilde{N_H}(0,f)$
Very thick oxide	$L \to \infty; A_H = 0$	$(1+j)\sqrt{\pi f D_H}$
Finite thickness: Hydrogen barrier at L	$\Phi_H(L,t) = 0$	$(1+j)\sqrt{\pi f D_H} \tanh\left((1+j)\sqrt{\pi f/D_H}L\right)$
Finite thickness: Free hydrogen at L	$N_H(L,t) = 0$	$(1+j)\sqrt{\pi f D_H} \coth\left((1+j)\sqrt{\pi f/D_H}L\right)$

of the aging tests are presented in [2, 5]. For the validation of the new aging model, here we chose to illustrate with the stress conditions P2 and P3 (above BV_{CE0} with V_{CE} = 2V, J_C =5 mA/µm^2 and V_{CE} = 3V, J_C =1 mA/µm^2, respectively) [2, 5]. Pre-stress parameter extraction were performed by an initial model calibration using a foundry generated scalable model card. Post-stress I_{REpS} values have been extracted from the low-V_{BE} region of the measured Gummel characteristics at each aging interval using the initial model card. Figure 6(a) compares the evolution of I_{REpS} under the two stress conditions, P2 and P3, between the aging model simulation and the extracted values (from measured forward Gummel characteristics), depicting good model accuracy. Once the accuracy of the principal aging model parameter, I_{REpS}, is validated, Fig. 6(b) compares the aging model simulation results with measurements for the Gummel plots under P2 stress condition at different stress intervals (0, 1, 3, 7, 72, 1000h) as a final model validation. Very good agreement between measurement and simulation at all aging times can be observed.
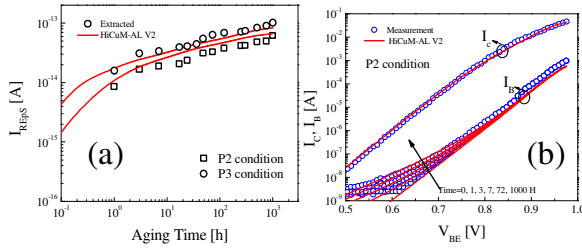

Fig. 6: Comparison between measurement and HiCuM-AL-V2 model simulation: (a) I_{REpS} under P2 and P3 conditions, and (b) Gummel plots under P2 stress condition.

3.2 Technology 2

The devices under test are NPN SiGe HBTs [17] based on an advanced BICMOS 55nm technology from STMicroelectronics featuring devices with a drawn emitter size of 0.2×5 µm² in CBEBC configuration. Transistors featuring low breakdown voltages are studied and DC test structures have been submitted to aging tests for 120h. The bias stress condition (V_{CB}=1.5V, J_E=8mA/µm², T=25°C as shown Fig. 7 (a)) are chosen above BV_{CEO} to accelerate the degradation mechanism. In [14], it was shown by a separation of the intrinsic and peripheral contributions of the base current that only the perimeter component is impacted by stress. This reaffirms that, alike technology 1 (and technology 3), the origin of the degradation mechanisms in these

HBTs are in the B-E periphery, adhering to classical hot-carrier degradation physics. Fig. 7 (b) shows the evolution of the I_{REpS} parameter under the stress conditions, $J_{E,stress}$=8 mA/µm², and $V_{CB,stress}$=1.5V comparing model simulation and extracted values from the measured Gummel plot, depicting a very good model accuracy. Next, in Fig. 7(c), model simulation and measurements are compared for the evolution of normalized excess base current ($\Delta I_B/I_{B0}$) with aging time, illustrating good model accuracy at V_{BE} = 0.5 and 0.6 V. A final validation is performed through simulation of the Gummel plot (Fig. 7(d)) employing both a foundry-generated scalable model card and the extracted aging model parameters, showing good agreement between the measurement and the simulation.
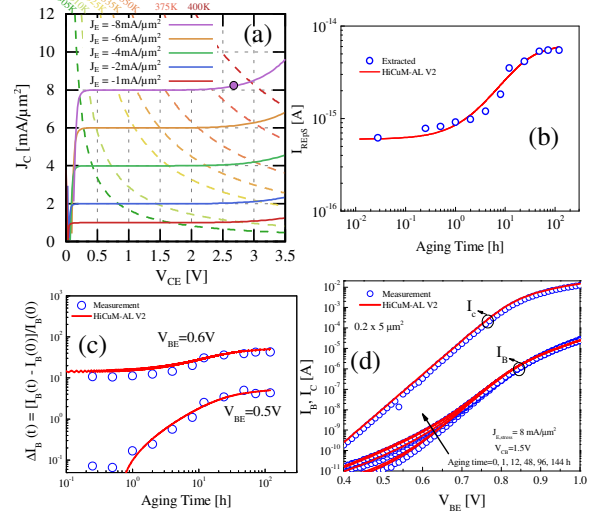

Fig. 7: (a) Aging test bias conditions for technology 2; Comparison between measurement and HiCuM-AL-V2 model simulation: (b) I_{REpS}, (c) normalized excess base current and (d) Gummel plots at different aging intervals.

Next the model validation was extended under dynamic mixed-mode stress conditions, similar to what has been illustrated in Fig. 1. For this, HBTs from technology 2 were subjected to two mixed-mode stress scenarios illustrated in Fig. 8: (i) in the first phase of duration 18h a C-B stress voltage of 1.5V has been applied followed by a higher stress bias of 2.2V for another 18h, followed by a final stress phase of 18h under a V_{CB} of 1.5V (same as phase 1); (ii) in the first phase of duration 18h, a V_{CB} stress of 1.6V has been applied followed by a higher stress bias of 2.1V for another 18h, followed by a final stress phase of 18h under a V_{CB} of 1.6V. While

the dynamics of the two cases are different due to different V_{CB} values, in both cases a pseudo-recovery phase can be observed in the last 18h due to a reduction in the stress voltage compared to phase 2 under stress 2. Note that, even though for scenario (i) (in red) a higher V_{CB} results in a higher degradation of I_{REpS} in phase 1, due to a higher V_{CB} in phase 2, scenario (ii) (in blue) shows a higher degradation of I_{REpS}. In both cases the model simulation have been compared with the extracted I_{REpS} values depicting very good model accuracy thus validating the model under dynamic operating conditions.
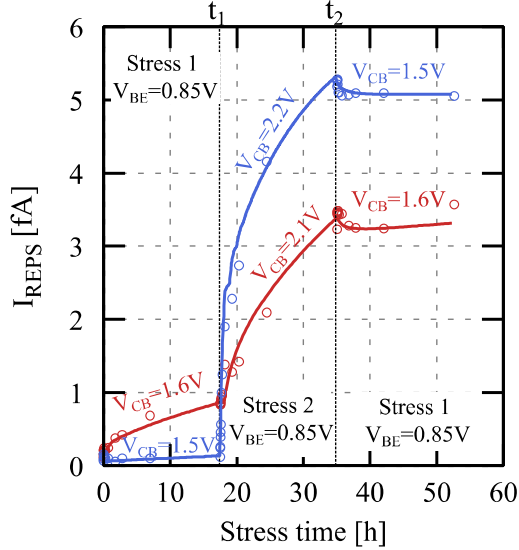

Fig. 8: Evolution of I_{REpS} for technology 2 under two dynamic stress conditions comparing the measurements (symbols) and HiCuM-AL V2 (line).

3.3 Technology 3

The aging model was finally validated on SG13S IHP technology [18] featuring transistors in BEC configuration with an effective emitter area of $8\times0.16\times0.52$ µm². Aging tests were performed under various mixed-mode stress conditions as presented in [2-4]. Corresponding stress bias conditions are presented in Fig. 9 highlighting a very large spectrum of aging tests allowing analysis of hot-carrier degradation governed by the two accelerating factors: V_{CB} and J_E. In all cases, aging tests were performed up to 1000h of stress time.
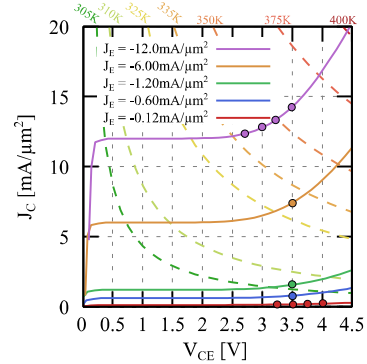

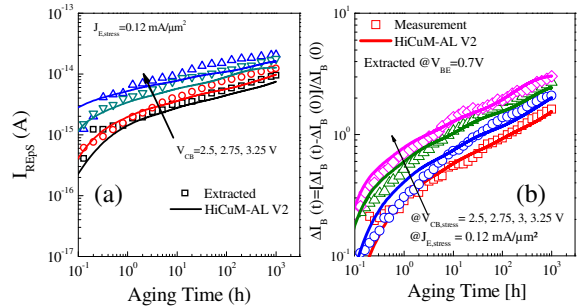Fig. 9: Aging test bias conditions for technology 3.

Fig. 10: Comparison between measurement and HiCuM-AL-V2 simulation: (a) I_{REpS} and (b) excess base current ($\Delta I_B/I_{B0}$) under $J_{E,stress}$ of 0.12, mA/µm² for different $V_{CB,stress}$.

For aging model validation, primarily a specific set of DC mixed-mode stress-conditions has been chosen among the cases illustrated in [2]: a $J_{E,stress}$ of 0.12 mA/µm² under different $V_{CB,stress}$ (2.5, 2.75, 3 and 3.25 V). Figs. 10 (a) and (b) show the evolution of the I_{REpS} parameter and the normalized excess base current ($\Delta I_B/I_{B0}$) as a function of aging time. Initial simulation is performed using a foundry-generated scalable model card followed by re-simulations using extracted aging model parameters, for different aging intervals. Good agreement between model and measurement is observed for all stress conditions. Next, the model validation has been performed under dynamic mixed-mode stress conditions on technology 3. A specific DC mixed-mode stress condition was chosen as a reference for this analysis: $I_{E,stress}$ of 0.12 mA under a $V_{CB,stress}$ of 3V. The normalized excess base current ($\Delta I_B/I_{B0}$) has been monitored over a period of 4000 s as shown in Fig. 11 (in blue). For the dynamic mixed-mode condition, both V_{CB} and I_E switch in an interval of 360s, between the initial ($V_{CB,stress}$ of 3V and $I_{E,stress}$ of 0.12 mA) and a high-current recovery phase ($V_{CB,stress}$ of

0V and a $I_{E,stress}$ of 5.2 mA at 3 times the current at

TABLE II: AGING PARAMETERS FOR THREE SiGe HBT TECHNOLOGIES

Tech	C_{MM} (s^{-1})	μ (V^{-1})	J_{Ehc} (mAµm^{-2})	ε	K_{R0} (cmA^{-1}s^{-1})	R_{10} (cm^{-1}s)	C_{10} (cm)	G_0 (cms^{-1})
1	3.8×10^{-6}	1.5	145	-0.35	10^{11}	60	0.4	8×10^{-6}
2	4.8×10^{-6}	1.2	145	-0.15	10^{10}	60	0.4	1×10^{-9}
3	7.5×10^{-7}	2.1	205	-0.35	10^{12}	60	0.4	3×10^{-3}

peak-f$_T$).

In case of dynamic stress, a significant recovery can be observed during the high- current phase (Fig. 11), owing to the annealing effect during this phase. Compared to the DC case, the dynamic case shows a smaller overall degradation, while at the first stress phase (at identical stress bias) both cases coincide. The aging model simulation has been compared to both measurements depicting good model accuracy in either cases. While the degradation phases under both DC and dynamic stress conditions (e.g. the first 360s of both cases) show identical values of the rate constants, $K_{F,I}$ and $K_{R,I}$, interestingly, the recovery phase shows an elevated value of the recombination rate constant $K_{R,I}$, while the $K_{F,I}$ value diminishes. Due to the annealing effect in the recovery phase, the generation rate ($K_{F,I}$) decreases and recombination rate ($K_{R,I}$) increases owing to increased passivation of interface traps by the hydrogen at the elevated temperature. It is important to note the absence of significant recovery in both cases depicted in Figs. 1 and 8 in comparison to that of Fig.11. This again affirms the fact that only with annealing or under temperature treatment the recovery can become significant in SiGe HBTs.

dynamic mixed-mode stress conditions comparing the measurements (symbols) and HiCuM-AL V2 (line).

3.4 Model Parameters

The general observation while extracting the aging model parameters is that forward rate constant, $K_{F,I}$, increases with $V_{CB,stress}$ following an exponential dependence while $J_{E,stress}$ is kept constant, On the other hand, while $V_{CB,stress}$ is kept constant, $K_{F,I}$ demonstrates a peak value before starting to roll off. This is consistent with the behavior observed previously [2-4]. This has been explained by a decrease in the C-B electric field at the onset of the Kirk effect at such high stress current densities [2, 4, 12], resulting in a reduction in ΔI_B. An empirical expression is valid for $K_{F,I}$ similar to the one proposed in [2, 4],

$$K_{F,I} = C_{MM} \exp(\mu V_{CB,stress})\left[\frac{1}{|J_{E,stress}|} + \frac{|J_{E,stress}|}{J_{Ehc}}\right]^{\varepsilon} \quad (16)$$

On the other hand, we observe a very weak bias dependence of the parameter $K_{R,I}$ and its evolution is principally dominated by temperature. This has also been observed in our previous work [2] where much smaller values of the bias-related coefficients ($C_{MM,R}$, μ_R, J_{Ehc}), had been extracted compared to that of $K_{F,I}$. Hence we have modified this equation in the sense that

$K_{R,I}$ is solely governed by junction temperature. Thus, the trap annihilation now follows an Arrhenius law,

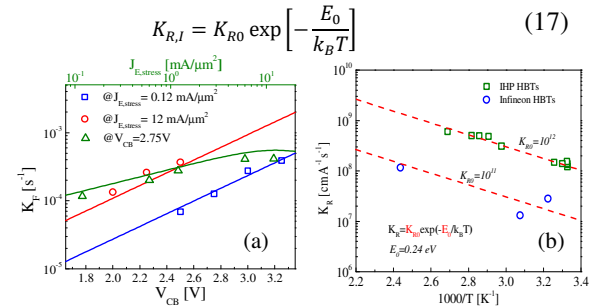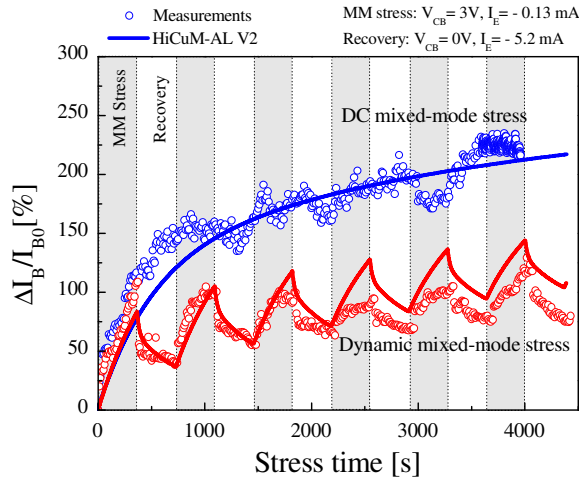$$K_{R,I} = K_{R0} \exp\left[-\frac{E_0}{k_B T}\right] \quad (17)$$

Fig. 12: Evolution of (a) $K_{F,I}$ for different $V_{CB,stress}$ and $J_{E,stress}$ and (b) $K_{R,I}$ as a function of the inverse of junction temperature.

Figure 12 shows extracted values of the generation-annihilation rate constants ($K_{F,I}$ and $K_{R,I}$) plotted as a function of the stress bias and inverse of temperature, respectively. Here, the values chosen to fit the $K_{F,I}$ in Fig. 12 (a) are C_{MM} =7.8×10⁻⁷s⁻¹, degradation acceleration exponential factor μ_0=2.75V⁻¹, empirical fit factor J_{Ehc}=155 mA/µm² and power exponent ε = -0.35. The activation energy, E_0, can also be extracted (Fig. 12(b), shown for both the IHP and Infineon technologies), resulting in an identical value of 0.24 eV for all technologies. This is logically consistent to the fact that both technologies employ the same Si/SiO₂ system, while the magnitudes differ due to a difference in device dimensions. Due to the diversity of stress conditions, many junction temperatures have been investigated allowing extraction of temperature dependence for the H⁺ diffusion parameter D_H. This parameter has a physical meaning since the diffusion of H⁺ atoms is accelerated by the temperature regardless of the technology features. Figure 13 presents the extracted values of D_H the three technologies under test plotted as a function of the inverse of junction temperature. It shows a general Arrhenius law (18) for D_H (T_j) with an excellent accuracy:

$$D_H = D_0\exp(-E_A/k_B T_j) \qquad (18)$$

with the activation energy E_A and the hydrogen diffusion constant D_0 at T_j=T_0. The extracted parameter values are close to the values reported in [19]. The temperature dependence of D_H directly influences the parameters R_1 and C_1 following eq. (13) as well as the terminal conductance G. However, it requires an activation energy, E_0, related to the trap features (similar to that of $K_{R,I}$), to describe temperature dependence of the R-C network parameters similarly to (18), as follows,

$$R_1 = R_{10}\exp(-E_0/k_B T_j),$$
$$C_1 = C_{10}\exp(-E_0/k_B T_j), \qquad (19)$$
$$\text{and } G = G_0\exp(-E_0/k_B T_j).$$

We observe that all the new parameter values E_0, R_{10} and C_{10} are identical regardless of the technology, which is consistent since they describe the same H-diffusion dynamics of Si/SiO₂ system. However, G_0 changes from one technology to another since it is governed by the final trap number. Finally using eqns. (16)-(19), we can now obtain a unique aging parameter set for each technology, as listed in table II, which is even more convenient from a design point-of-view.
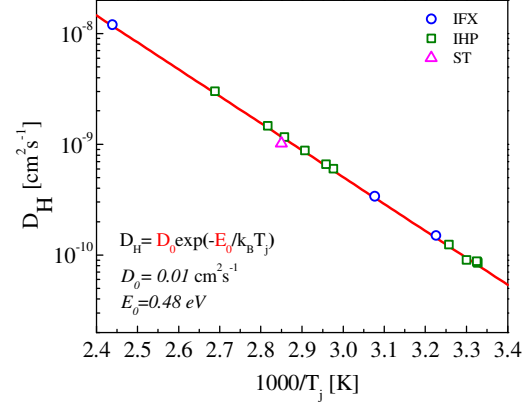

Fig. 13: General form of the temperature dependence of the hydrogen diffusion parameter D_H for the three technologies under test.

4. Conclusion

In this work, we have presented a new physical and accurate aging compact model implementation for modern SiGe HBTs based on the reaction-diffusion theory of hot-carrier degradation and a differential form of Fick's law of diffusion. The model implementation, although complex compared to its predecessor while employing additional transistor nodes in simulation, ensures invariance in time of the degradation characteristics. The aging model has been compared with long-term aging tests on various SiGe HBT technologies, yielding very good agreement thus confirming its accuracy and versatility. The proposed model formulation can easily be co-integrated with existing circuit design framework. With its strong physical basis, the proposed model can prove to be indispensable for ensuring stable circuit operation close to the SOA of the technology, through prediction of reliability-aware circuit architectures.

References

[1] P. Chevalier, M. Schröter, C. R. Bolognesi, V. d'Alessandro, M. Alexandrova, J. Böck, R. Flückiger, S. Fregonese, B. Heinemann, C. Jungemann, R. Lövblom, C. Maneux, O. Ostinelli, A. Pawlak, N. Rinaldi, H. Rücker, G Wedel and T. Zimmer, "Si/SiGe:C and InP/GaAsSb Heterojunction Bipolar Transistors for THz Applications," *Proc. IEEE*, vol. 105, no. 6, pp. 1035-1050, June 2017, DOI: 10.1109/JPROC.2017.2669087.

[2] C. Mukherjee, T. Jacquet, G. G. Fischer, T. Zimmer, and C. Maneux, " Hot Carrier Degradation in

SiGeHBTs: A Physical and Versatile Aging Compact Model," IEEE Transactions on Electron Devices, vol. 64, no. 12, pp. 4861-4867, Dec. 2017.DOI: 10.1109/TED.2017.2766457.

[3] G. G. Fischer and G. Sasso, "Ageing and thermal recovery of advanced SiGe heterojunction bipolar transistors under long-term mixed-mode and reverse stress conditions," *Microelectron. Reliab.* vol. 55, no. 3, pp. 498–507, Mar. 2015, DOI: 10.1016/j.microrel.2014.12.014.

[4] G. G. Fischer, "Analysis and modeling of the long-term ageing rate of SiGe HBTs under mixed-mode stress," 2016 *IEEE Bipolar/BiCMOS Circuits and Technology Meeting* (BCTM), NJ, 2016, pp. 106-109, DOI: 10.1109/BCTM.2016.7738958.

[5] T. Jacquet, G. Sasso, A. Chakravorty, N. Rinaldi, K. Aufinger, T. Zimmer, V. d'Alessandro and C.Maneux, "Reliability of high-speed SiGe: C HBT under electrical stress close to the SOA limit," *Microelectron. Reliab.* vol. 55, no. 9, pp. 1433–1437, 2015, DOI: 10.1016/j.microrel.2015.06.092.

[6] G. Zhang, J. D. Cressler, G. Niu and A. J. Joseph, "A new "mixed-mode" base current degradation mechanism in bipolar transistors," *Proc. BCTM* Minneapolis, USA, 2002, pp. 32-35. doi: 10.1109/BIPOL.2002.1042881

[7] J. D. Cressler, "Emerging SiGe HBT reliability issues for mixed-signal circuit applications," *IEEE Trans. Device Mater. Rel.* vol. 4, no. 2, pp. 222–236, Jun. 2004, DOI: 10.1109/TDMR.2004.826587.

[8] H. Kamrani, D. Jabs, V. d'Alessandro, N. Rinaldi, T. Jacquet, C. Maneux, T. Zimmer, K. Aufinger, and C. Jungemann, "Microscopic Hot-Carrier Degradation Modeling of SiGe HBTs under Stress Conditions Close to the SOA limit", *IEEE Trans. Electron Dev.*, vol. 64, pp. 923-929, 2017, DOI: 10.1109/TED.2017.2653197.

[9] C. Mukherjee, B. Ardouin, J. Y. Dupuy, V. Nodjiadjim, M. Riet, T. Zimmer, F. Marc, and C. Maneux, "Reliability-Aware Circuit Design Methodology for Beyond-5G Communication Systems," *IEEE Trans. Device Mater. Rel.* vol. 17, no. 3, pp. 490-506, *Sept. 2017*, DOI: 10.1109/TDMR.2017.2710303.

[10] K. O. Jeppson and C. M. Svensson, "Negative bias stress of MOS devices at high electric fields and degradation of MNOS devices," *J. Appl. Phys.*, vol. 48, pp. 2004–2014, 1977, DOI: 10.1063/1.323909.

[11] A. E. Islam, H. Kufluoglu, D. Varghese, S. Mahapatra and M. A. Alam, "Recent Issues in Negative-Bias Temperature Instability: Initial Degradation, Field Dependence of Interface Trap Generation, Hole Trapping Effects, and Relaxation," *IEEE Trans. Electron Dev.*, vol. 54, no. 9, pp. 2143-2154, Sept. 2007, DOI: 10.1109/TED.2007.902883.

[12] B. R. Wier, K. Green, J. Kim, D. T. Zweidinger, and J. D. Cressler, "A physics-based circuit aging model for mixed-mode degradation in SiGe HBTs," *IEEE Trans. Electron Dev.*, vol. 63, no. 8, pp. 2987–2993, Aug. 2016, DOI: 10.1109/TED.2016.2573263.

[13] A. J. Scholten, D. Stephens, G. D. J. Smit, G. T. Sasse and J. Bisschop, "The Relation Between Degradation Under DC and RF Stress Conditions," *IEEE Transactions on Electron Devices*, vol. 58, no. 8, pp. 2721-2728, Aug. 2011. doi: 10.1109/TED.2011.2153854.

[14] M. Jaoul, D. Ney, D. Céli, Cristell Maneux and T. Zimmer, "Analysis of a failure mechanism occurring in SiGe HBTs under mixed-mode stress conditions", *IEEE ICMTS*, Fukuoka, Japan, 2019, pp. 33-37. doi: 10.1109/ICMTS.2019.8730951.

[15] M. Schröter and A. Chakravorty, "Compact hierarchical modeling of bipolar transistors with HICUM", World Scientific, Singapore, ISBN 978-981-4273-21-3, 2010.

[16] M. Couret, G. Fischer, S. Frégonèse, T. Zimmer, and C. Maneux, "Physical, small-signal and pulsed thermal impedance characterization of multi-fingers SiGe HBTs close to the SOA edges", *IEEE ICMTS*, Fukuoka, Japan, 2019, pp. 154-159. doi: 10.1109/ICMTS.2019.8730964.

[17] P. Chevalier, G. Avenier, G. Ribes, A. Montagné, E. Canderle, D. Céli, N. Derrier, D. Ney, J. Rosa, "A 55 nm triple gate oxide 9 metal layers SiGe BiCMOS technology featuring 320 GHz f_T/ 370 GHz f_{MAX} HBT and high-Q millimeter-wave passives," 2014 IEEE International Electron Devices Meeting, San Francisco, CA, 2014, pp. 3.9.1-3.9.3. doi: 10.1109/IEDM.2014.7046978

[18] H. Rucker B. Heinemann, W. Winkler, R. Barth, J. Borngräber, J. Drews, G. G. Fischer, A. Fox, T. Grabolla, U. Haak, Di. Knoll, F. Korndörfer, A. Mai, S. Marschmeyer, P. Schley, D. Schmidt, J. Schmidt, M. Andreas Schubert, K. Schulz, B. Tillack, D. Wolansky, and Y. Yamamo, "A 0.13μm SiGe BiCMOS Technology Featuring f_t/f_{max} of 240/330 GHz and Gate Delays Below 3 ps," *IEEE J. Solid-State Circuits*, vol. 45, no. 9, pp. 1678–1686, Sep. 2010, DOI: 10.1109/JSSC.2010.2051475.

[19] U. S. Raghunathan, P. S. Chakraborty, T. G. Bantu, B. R. Wier, H. Yasuda, P. Menz, and J. D. Cressler, "Bias- and temperature-dependent accumulated stress modeling of mixed-mode damage in SiGe HBTs," *IEEE Trans. Electron Devices*, vol. 62, no. 7, pp. 2084–2091, Jul. 2015, DOI: 10.1109/TED.2015.2433299.